GA–A25576

PEDESTAL PERFORMANCE DEPENDENCE UPON PLASMA SHAPE IN DIII-D

by
A.W. LEONARD, T.A. CASPER, R.J. GROEBNER,
T.H. OSBORNE, P.B. SNYDER, and D.M. THOMAS

OCTOBER 2006

GENERAL ATOMICS

DISCLAIMER

GA–A25576

PEDESTAL PERFORMANCE DEPENDENCE UPON PLASMA SHAPE IN DIII-D

by
A.W. LEONARD, T.A. CASPER,* R.J. GROEBNER,
T.H. OSBORNE, P.B. SNYDER, and D.M. THOMAS

This is a preprint of a paper to be presented at the 21st IAEA Fusion Energy Conference, October 16-21, 2006, in Chengdu, China, and to be published in the *Proceedings.*

*Lawrence Livermore National Laboratory, Livermore, California.

Work supported by
the U.S. Department of Energy
under DE-FC02-04ER54698 and W-7405-ENG-48

GENERAL ATOMICS PROJECT 30200
OCTOBER 2006

Pedestal Performance Dependence Upon Plasma Shape

A.W. Leonard 1), T.A. Casper 2), R.J. Groebner 1), T.H. Osborne 1), P.B. Snyder 1), and D.M. Thomas 1)

1) General Atomics, San Diego, California, USA
2) Lawrence Livermore National Laboratory, Livermore, California, USA

e-mail contact of main author: Leonard@fusion.gat.com

Abstract. Higher moments of the plasma shape than triangularity are found to significantly affect the pedestal pressure and edge localized mode (ELM) characteristics in DIII-D. The shape dependence of the pedestal pressure was experimentally examined by varying the squareness in the proposed ITER configuration while holding the triangularity fixed. Over this scan the pedestal pressure increased by ~50% from highest squareness to lowest squareness. The ELM energy also varied with the shape to maintain a nearly constant fraction of the pedestal energy. Stability analysis of model shapes and pressure profiles indicates that much of the advantage of high triangularity for high pedestal pressure can be achieved by optimizing squareness and/or the distance of the secondary upper separatrix from the primary separatrix. The variation in pedestal energy with squareness was also used to optimize "Hybrid" discharges in DIII-D. In the "Hybrid" regime low squareness resulted in a high pedestal pressure with large infrequent ELMs that eventually triggered an internal 2/1 tearing mode that locked, resulting in a disruption. At higher squareness the pedestal pressure was reduced with smaller and more rapid ELMs, resulting in control of the total stored energy and maintenance of a steady beneficial internal 3/2 tearing mode. For both the ITER and hybrid discharges an increase in pedestal width at low squareness appears to be a significant factor in the increase in total pedestal pressure.

1. Introduction

The edge H-mode pedestal plays a key role in several important aspects of tokamak operation including global confinement and surface heat flux transients due to edge-localized-modes (ELMs). Tokamak confinement increases with higher pedestal pressure in regimes of stiff core transport and a robust pedestal is expected to be necessary for ITER to achieve its performance objectives [1-3]. However, larger ELMs typically result from a higher pressure pedestal, resulting in transients potentially damaging to plasma facing components, and triggering instabilities such as neo-classical tearing modes [4,5]. Control of the pedestal, in design and operation, is therefore critical for optimization of tokamak performance.

While it has long been recognized that a high triangularity shape allows a higher pedestal pressures through a higher edge MHD stability limit [3,6-10], higher moments of the plasma shape can also affect the edge MHD stability limit and change the pedestal pressure at the onset of ELMs. In DIII-D a scan of squareness in a double-null configuration produced a wide range of pedestal pressure for otherwise similar conditions [11,12]. For plasma control squareness has an advantage over triangularity in that the divertor configuration can remain nearly fixed as the shape is modified. This is important for the closed divertor configurations planned for future reactor-sized tokamaks where pumping and density control are highly dependent on the divertor geometry.

Here we report on experimental data and stability analysis of scans of plasma squareness with fixed triangularity in DIII-D. Section 2 describes a squareness scan in a lower single-null configuration similar to the proposed ITER shape where a 50% increase to the pedestal height is obtained by modifying the shape of the upper half of the plasma. Section 3 examines the MHD stability of the pedestal and finds consistency with the shape scan experimental results. Other aspects of shape variations are also explored with modeling. Section 4

describes the effect of squareness on a higher triangularity hybrid configuration where the highest pedestal pressure and global confinement is not always optimum for overall performance. Section 5 follows with discussion and implications of these results.

2. ITER Shape Scan

To assess the edge pedestal sensitivity to shape changes in an ITER-like geometry, a shaping experiment was carried out in DIII-D. The squareness of the upper half of the discharge was varied from 0.33 to 0.39, as shown in Fig. 1. For this report, squareness is defined as the extent of the separatrix in each quadrant between a triangle (sq=0) and a rectangle (sq=1.0). In the experimental scan at the highest upper-outer squareness the upper triangularity decreased somewhat so the lower triangularity was increased slightly to compensate. The average triangularity increased from $\langle\delta\rangle = 0.48$ at the highest squareness to $\langle\delta\rangle = 0.56$ at the lowest squareness. Another important aspect of the shape variation was the secondary upper x-point moved from well outside the vessel at the highest squareness to inside the vessel at the lowest squareness with a separation from the primary separatrix of 1.6 cm mapped to the outer midplane (DRSEP=1.6 cm).

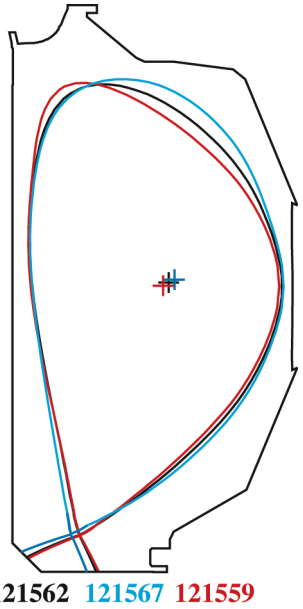

FIG. 1. Plasma equilibrium shapes used in the study. The central black curve represents the separatrix of the proposed ITER shape. The other shapes have either higher squareness (blue) or lower squareness (red) in the upper outer quadrant of the plasma shape.

The effect of shape variation was assessed in a standard H-mode with constant density and injected power. The discharge conditions were plasma current of 1.5 MA, toroidal field of 1.8 T for $q_{95} \sim 3.7$, with 6.8 MW of neutral beam injected power. The shape was scanned stepwise in a series of discharges, while other conditions were kept constant during the ELMing phase, including constant line-averaged density of approximately 6×10^{19} m^{-3}, or ~40% of the normalized Greenwald density. The pedestal profile is analyzed by collecting data from the last 20% of each ELM cycle for one second during constant conditions in each discharge. This phase of the ELM cycle is characterized to better assess edge stability just before ELM onset. The electron density and temperature profiles are measured every 12.5 ms by a Thomson scattering diagnostic with high spatial resolution in the edge plasma. The ion temperature is determined by a charge exchange recombination (CER) spectroscopy diagnostic measuring CVI ions. The ion density adjusted from the electron density by a carbon density measurement from the CER diagnostic. The profile data are all mapped onto the magnetic flux coordinate, ψ, and then fit with a tanh function for the pedestal region and polynomial function for the central core part of the profile. The total pressure is determined by combining the electron and ion profiles with corrections to the ion density from carbon density measurements. The fast ion pressure from neutral beam injection is also included, but contributes very little to the pedestal pressure.

The variation of fitted pedestal profiles with the shape scan is shown in Fig. 2. While the pedestal density just before an ELM remains roughly constant with the shape scan, both the electron and ion pedestal temperature increase with less squareness resulting in a higher pressure. The pressure at the top of the pedestal as a function of upper outer squareness is plotted in Fig. 3. The pedestal pressure increases by about 50% from the lowest squareness to the highest.

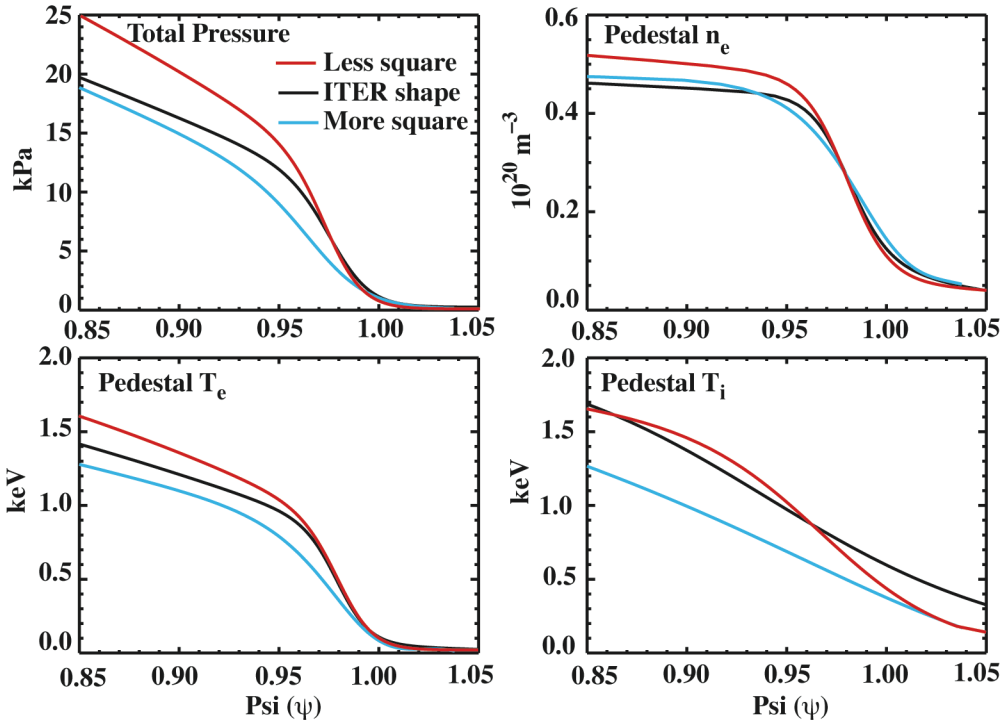

FIG. 2. The fitted pedestal profiles just before an ELM for the ITER shape and less and more square shapes. Shown are the (a) total pressure, (b) electron density, (c) electron temperature and (d) ion temperature.

Another important aspect of the pedestal is the ELM characteristics. Over the shape scan the energy lost at each ELM became larger as the pedestal increased with decreasing squareness, keeping the ELM energy roughly a fixed fraction of the pedestal energy at ~9% [11]. The ELM frequency also varied inversely with the pedestal height keeping the fraction of input power carried by ELMs constant. Squareness provides a relatively simple control to optimize the trade off between pedestal height and ELM size.

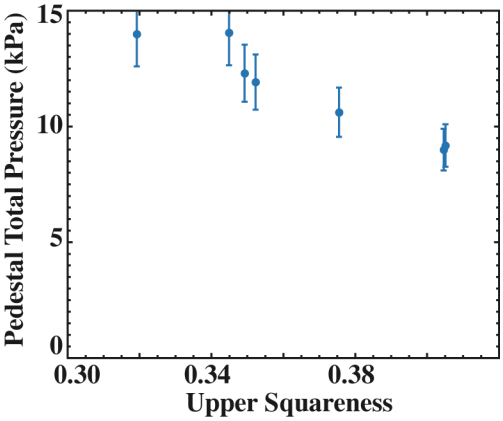

FIG. 3. The total pressure at the top of the pedestal as a function of upper outer squareness.

3. Stability Analysis

The edge stability of the discharges in the shape scan was analyzed to provide insight into the physics governing the variation of the pedestal pressure observed in the experiment and to gain confidence in projecting these results for future tokamaks. Analysis of the edge stability requires accurate description of the pedestal pressure and current profiles within the context of a magnetic equilibrium. All of the relevant profiles necessary for specifying the total pressure are mapped onto magnetic flux coordinates using an initial magnetic equilibrium constructing using magnetic and motional Stark effect (MSE) measurements. The edge current is specified by a neoclassical bootstrap current model [12] and a fully relaxed ohmic profile. The total pressure and edge current are then used as constraints for a full kinetic equilibrium reconstruction.

The code ELITE provides growth rates and eigenmode structure of edge peeling-ballooning modes based on the reconstructed kinetic equilibrium [13-15]. While the analysis can provide the growth rate for a specific experimental condition, further insight can be gained by mapping out the stability space around the operating point. The mapping is carried out by constructing a number of equilibria with variations in edge pedestal pressure and current. The edge pressure, $\Psi_{norm} > 0.8$, is varied by a constant factor while the interior pressure is adjusted to keep total stored energy constant. In a similar fashion the edge current is independently varied by a constant factor with the interior current adjusted to keep the total plasma current fixed. Stability analysis is carried out on each reconstructed equilibrium, a total of ~80, for toroidal modes of $n = 5$, 10, 20, 25, and 30. The growth rates of the most unstable mode from each equilibrium are collated to produce a 2D map of edge stability as shown in Fig. 4. In this figure, the growth rate, normalized to the Alfvén time, is plotted as a color contour as a function of the average pedestal current, normalized by the total average current density, and normalized pedestal pressure gradient [16]. The approximate stability boundary, $\gamma_E/\gamma_A = 0.1$ is delineated with a black contour line, while the measured pedestal pressure gradient, modeled current density and their uncertainties are shown with a black cross symbol. While the experimentally measured pressure gradient appears to exceed the stability boundary by ~20%, the actual gradient may be within the uncertainty of the measurement and modeled stability limit. The peak gradient is a particularly difficult measurement prone to larger uncertainty than the total pressure at the top of the pedestal.

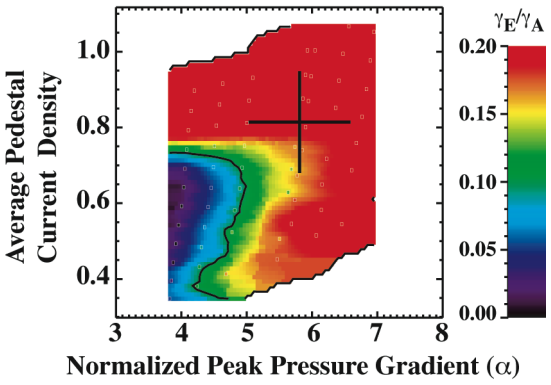

FIG. 4. Stability map for the pedestal in an ITER similar shape. The growth rate of the peeling-ballooning mode normalized to the Alfvén time is plotted as a color contour. The stability limit is approximately $\gamma_{ELM}/\gamma_A = 0.1$ as shown by the black curve. The experimentally measured operational location is shown by the "+" symbol.

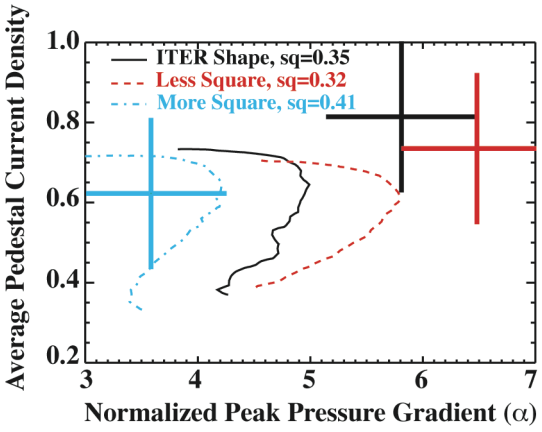

FIG. 5. Contours of stability, $\gamma_{ELM}/\gamma_A = 0.1$, for the ITER similar shape and more square and less square shapes. The experimental conditions are shown by the "+" symbols.

The stability boundary for the ITER shape is overlaid with the boundaries for the high and low squareness extremes of the shape scan in Fig. 5. The peak stable pressure gradient increases steadily with decreasing squareness while the maximum stable pedestal current density does not appear to change appreciably with shape. Within experimental uncertainty the experimental peak pressure gradient generally lies at the upper right corner of the stability boundary.

The maximum stable pressure gradient from each of the discharges produces a graph of stability limit versus shape as shown in Fig. 6. The curve labeled "stability limit" shows an

increase in the pressure gradient stability limit of 37% from highest squareness to lowest. The experimental pressure gradient exhibits the same trend with squareness within the experimental uncertainty. The more accurate measurement of the total pressure at the pedestal top increases 60% at low squareness. This larger pressure variation could still be consistent with the stability analysis if the pedestal becomes wider at lower squareness.

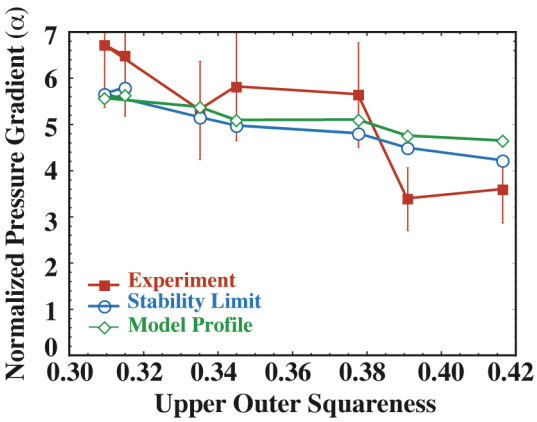

FIG. 6. Pedestal pressure gradients as a function of upper-outer squareness for (a) experimental measurements, (b) stability limit using the measured profiles and (c) stability limit using the ITER-shape experimental profile for all of the plasma shapes.

To separate out the effects of pedestal profile changes on the stability limit, the analysis was also carried using a single pressure profile shape as a model profile. The pressure and current profiles from the ITER-shaped discharge were used to constrain the magnetic equilibrium reconstruction for each of the shapes of the experimental scan. As before, equilibria with variations in edge pressure and current magnitude are constructed, but now with constant pedestal width across shapes. After stability analysis of each equilibria variation, similar to Fig. 4, the maximum stable pressure gradient for each shape is plotted in Fig. 6 with the label "model profile". For the model profile the maximum stable pressure gradient increases by 21% across the shape scan. This represents the expected change in total pedestal pressure across the shape scan if there are no changes to the pedestal profile shape. The similar trend for the fixed profile stability analysis indicates that changes to the pedestal width within the measurement uncertainty does not significantly affect the pressure gradient limit. The experimentally observed greater increase in total pedestal pressure could be explained by an increase in pedestal width at low squareness. The pedestal, or transport barrier, width could change with shape due to such effects as change in edge magnetic shear. A previous modeling study indicates that the total pedestal pressure limit scales with the pedestal width to the 0.7 power if all else is kept constant [15]. The increase in pedestal height with increasing width is somewhat less than linear because the typical unstable modes have eigenmodes with finite spatial extent and respond to the whole pedestal profile not just the highest local pressure gradient. An increase in pedestal width of ~45%, within the uncertainty of the measurement, could account for the observed 60% increase in pedestal height and still maintain consistency with the stability analysis. Because of the uncertainty of the width measurement further detailed experiments and analysis are needed to understand how the pedestal width responds to shape changes.

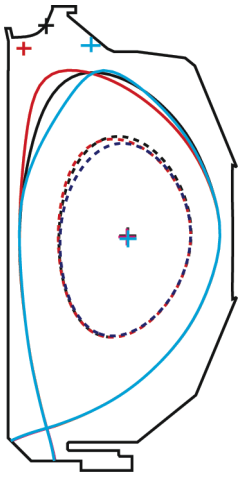

FIG. 7. Model shapes used in the pedestal stability study. The secondary X-point locations are also shown.

The results above motivate further studies of the shape of the upper half of a lower single-null discharge and its effect on pedestal stability. Three shapes were constructed, Fig. 7, for a range of upper triangularity and squareness. Operationally increasing the triangularity, or decreasing the squareness requires moving the upper secondary X-point closer to the primary

separatrix (lower DRSEP). A stability curve was constructed for each shape using the method described earlier, with the experimental pressure and modeled current profile from the ITER shaped discharge. The results of the stability analysis are shown in Fig. 8. In this analysis the maximum stable pressure increases by ~20% by increasing the upper triangularity from 0.25 to 0.47. The high triangularity shape also requires a smaller DRSEP (mapped to the midplane) of 1.3 cm. Much of the benefit of high triangularity can be realized simply by decreasing squareness, or DRSEP, while maintaining low triangularity. In this sample case the maximum stable pressure gradient increased by 10% by reducing DRSEP from 3.6 cm to 1.2 cm, even while decreasing the upper triangularity from 0.25 to 0.16. The upper outer squareness of these shapes decreased along with DRSEP. The results of this shape study are shown in Table I. The important physical aspect of shape for pedestal stability is related to the fraction of field line length in the pedestal that is in a good curvature region as opposed to bad curvature. The different shape parameters, triangularity, squareness and DRSEP capture aspects of this, but none completely, or uniquely. The shape studies presented here lend confidence that systematic studies can be used for design of plasma shape for optimal pedestal stability.

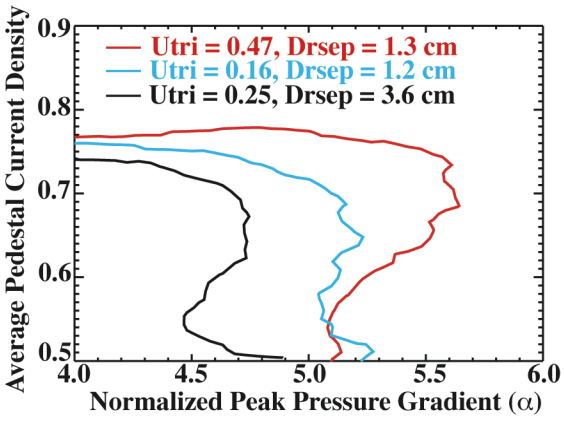

FIG. 8. Contours of stability, γ_{ELM}/γ_A = 0.1, for the shapes of Fig. 7 using a common pedestal profile.

Table I. Parameters of Shape Study

Upper Triangularity	DRSEP (cm)	Squareness	Peak Gradient (α)
0.27	4.7	0.374	4.7
0.50	2.0	0.357	5.6
0.16	1.9	0.330	5.2

4. Pedestal Optimization in Hybrid Discharges

Optimization of total discharge performance does not always occur for maximum pedestal pressure. This can be seen in operation of Hybrid discharges on DIII-D. hybrid discharges are regimes of improved H-mode confinement usually obtained with a flatter central current profile to avoid sawteeth [17]. Two discharges are shown in Fig. 9 which

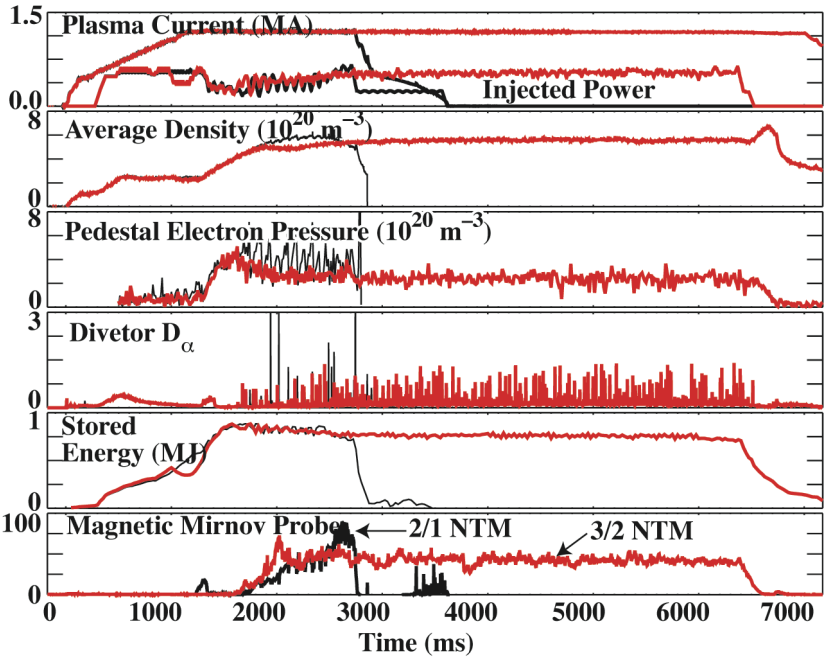

FIG. 9. Time traces for hybrid discharges at lower (black) and higher (red) squareness. Shown are (a) plasma current and injected power, (b) line-averaged density, (c) pedestal electron pressure, (d) divertor D_α emission, (e) total stored energy and (f) magnetic signals from internal tearing mode activity.

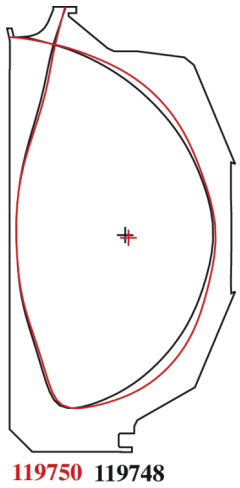

FIG. 10. Shapes for the hybrid discharges at lower squareness (black) and higher squareness (red).

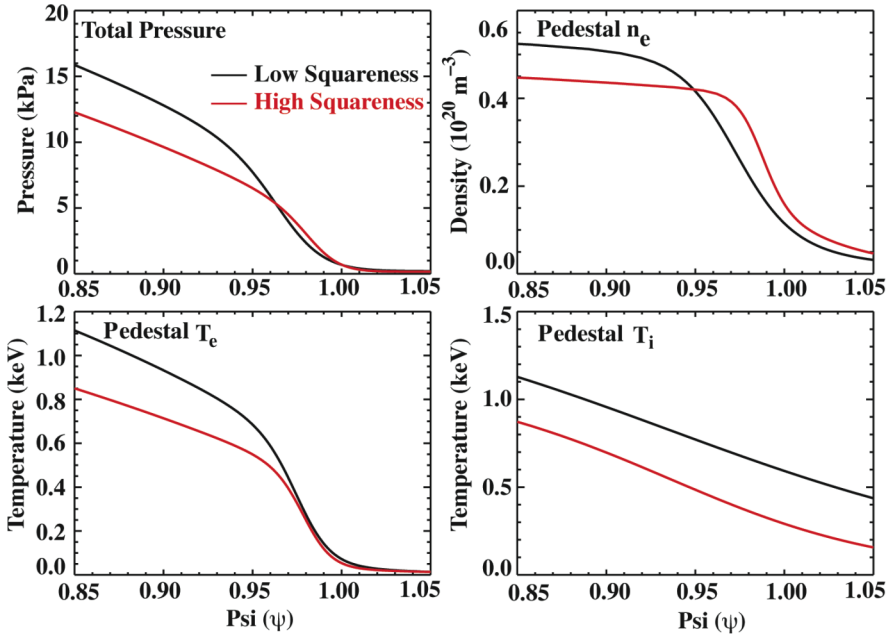

FIG. 11. Pedestal profiles for the lower squareness (black) and higher squareness (red) hybrid discharges. Shown are the (a) total pressure, (b) electron density, (c) electron temperature and (d) ion temperature.

only differ in their shape as shown in Fig. 10. For the low squareness shape the discharge terminates early because of a 2/1 neoclassical tearing mode (NTM) that grows and then locks to the wall destroying confinement. The NTM is triggered by large ELMs and high β resulting from good confinement. With higher squareness a lower pedestal pressure is attained with smaller and more frequent ELMs. Although the global confinement is somewhat lower, the discharge can be maintained with high β ($\beta_N \sim 2.6$) and still improved confinement ($H_{L89} \sim 2.1$). In high squareness, a relatively benign 3/2 NTM is initiated and saturates instead of the deleterious 2/1 mode.

Changes in pedestal pressure and ELM characteristics with squareness in the hybrid discharges are consistent with stability analysis. The profiles just before an ELM for the two shapes are shown in Fig. 11. The pedestal pressure is higher by ≈70% with both the gradient and width of the pedestal pressure increasing. Stability analysis for these discharges and measured profiles was carried out in the same manner described above with the results shown in Fig. 12. The maximum stable pressure gradient increases ~25% and the measured pressure gradient increase is similar. As

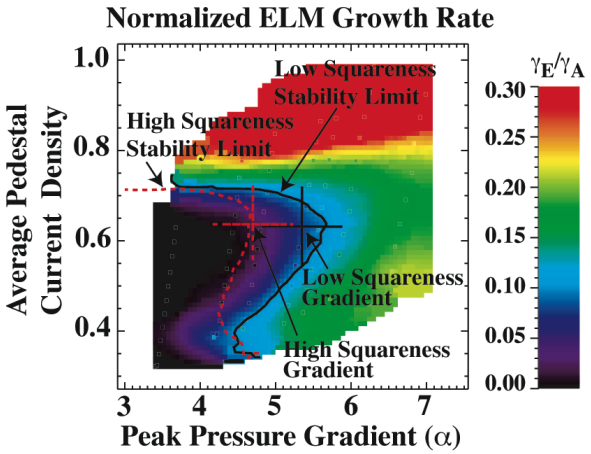

FIG. 12. The edge stability map for low squareness hybrid discharge. The stability boundary contour for $\gamma_{ELM}/\gamma_A = 0.1$ is shown by the black curve. The stability boundary contour for the higher squareness discharge is shown by the red curve.

in the previous ITER shaped case, it appears that the pedestal width may increase with decreasing squareness. This example shows that small changes in shape can lead to significant increases in discharge performance.

5. Summary

Higher moments of the plasma shape than triangularity, particularly squareness, have been shown to modify the edge stability limit and pedestal height. Lower squareness in the upper outer shape of a lower single-null configuration can increase the pedestal pressure. Accompanying the higher pedestal is an increase in ELM energy proportional to the increase in pressure. The increase in pedestal pressure is consistent with a calculation of the stability limit of the edge plasma versus shape. There are also indications the pedestal plasma increases in width at lower squareness. A study of shape variations with a model pressure profile showed that the expected benefit from changes to the upper half of the plasma can be accurately calculated. Details of the shape, including triangularity, squareness and the location of the secondary separatrix, can all play a role in determining the pedestal pressure in a single-null configuration plasma. For overall plasma performance, however, the optimal pedestal plasma is not always the highest pedestal pressure. In hybrid discharges in DIII-D, a somewhat lower pedestal pressure, through increased squareness, produces smaller ELMs and deleterious tearing modes can be avoided resulting in sustainment of a high performance plasma. Use of higher moments of the plasma shape, such as squareness, offers control of the pedestal without disturbing the divertor configuration and associated features of pumping, fueling and heat flux control. Such modest shaping flexibility in ITER could offer significant benefits in discharge performance.

This work was supported by the U.S. Department of Energy under DE-FC02-04ER54698 and W-7405-ENG-48.

References

[1] HUBBARD, A.E., Plasma Phys. Control. Fusion **42** (2000) A15.
[2] HATAE, T., SUGIHARA, M., and HUBBARD, A.E., Nucl. Fusion **41** (2001) 285.
[3] OSBORNE, T.H., *et al.,* Plasma Phys. Control. Fusion **42** (2000) A175.
[4] ZOHM, H., Plasma Phys. Control. Fusion **38** (1996) 105.
[5] JANESCHITZ, G., J. Nucl. Mater. **290–293** (2001) 1.
[6] SAIBENE, G., *et al.,* Nucl. Fusion **39** (1999) 1133.
[7] KAMADA, Y., *et al.,* Plasma Phys. Control. Fusion **41** (1999) B77.
[8] STOBER, J., *et al.*, Plasma Phys. Control. Fusion **42** (2000) A211.
[9] SNYDER, P.B., *et al.,* Nucl. Fusion **44** (2004) 320.
[10] SNYDER, P.B., *et al.,* Plasma Phys. Control. Fusion **46** (2004) A131.
[11] FERRON, J.R., *et al.,* Phys. Plasmas **7** (2000) 1976.
[12] FERRON, J.R., *et al.,* Nucl. Fusion **40** (2000) 1411.
[13] LEONARD, A.W., *et al.,* Phys. Plasmas **10** (2003) 1765.
[14] SAUTER, O., ANGIONI, C., and LIN-LIU, Y.R., Plasmas **6** (1999) 2834.
[15] WILSON, H.R., *et al.,* Phys. Plasmas **9** (2002) 1277.
[16] MILLER, R.L., *et al.,* Phys. Plasmas **5** (1998) 978.
[17] WADE, M.R., *et al.,* Nucl. Fusion **45** (2005) 407.